

# Effect of shear angle in shearing on stretch flangeability of ultra-high strength steel sheets

YAGITA Ryo<sup>1,a \*</sup>, KIMURA Shunsuke<sup>1,b</sup> and ABE Yohei<sup>1,c</sup>

<sup>1</sup>Toyohashi University of Technology, 1-1, Hibarigaoka, Tempaku, Toyohashi, Aichi 441-8580 Japan

<sup>a</sup>yagita@plast.me.tut.ac.jp, <sup>b</sup>kimura@plast.me.tut.ac.jp, <sup>c</sup>abe@plast.me.tut.ac.jp

**Keywords:** Stretch Flangeability, Ultra-High Strength Steel Sheets, Shearing

**Abstract.** The effect of the shear angle in shearing on the stretch flangeability of 980 MPa ultra-high strength steel sheets was examined. The sheared edges of the ultra-high strength steel sheets sheared at different shear angles were investigated, and then the cracking on the sheared edge after stretch flanging was observed. The length of the fracture surface in the sheared edge was decreased by shearing with the punch with a shear angle, whereas many cracks and burrs at the edge of the fracture surface were caused, and the boundary between the burnished and fracture surfaces became rougher. In stretch flanging, the cracks in the fracture bottom side rapidly increased with the bending length. The stretch flangeability increased at a shear angle, where the number of cracks per unit length was the highest, i.e. this indicates that the large number of cracks in the sheared edge were effective in suppressing penetration cracking to fracture in the stretch flanging.

## Introduction

To improve the fuel consumption of automobiles, the reduction in weight is intensively required in the automobile industry. To reduce the weight, the application to automotive parts using high strength and ultra-high strength steel sheets increases. The ultra-high strength steel sheet having a tensile strength above 1000 MPa is effective for automotive parts. However, in cold stamping of ultra-high strength steel sheets, there are many resolving problems such as large stamping load [1], large springback [2], low formability [3], tool failure [4] and hydrogen-induced delayed fracture [5].

Steel sheets are typically cut by shearing, and then are formed by stamping to the parts. When steel sheets are bent into a concave shape in stamping, tensile stress are generated at the concave shape edges. Because the sheared edge of the sheet has large plastic deformation and fracture in shearing, the sheared edge qualities was usually changed. Yagita et al. [6] showed that the sheared edge of the ultra-high strength steel sheets was affected by the shear angle in the punch and the blankholding force. The sheared edge qualities for edge cracking in the hole expansion [7] and the stretch flange abilities [8] were investigated. Sartkulvanich et al. [9] showed that the damage value is related to the blanking clearance in the hole expansion of 590 MPa steel sheet.

On the other hand, the studies have been performed to improve stretch flanging ability through material composition and crystalline structure. Pan et al. [10] produced 780 MPa steel sheet with different compositions and showed that stretch flangeability was affected by the strength difference between ferrite and martensite, and that the addition of Nb could increase ferrite strength and improve stretch flangeability. Gwon et al. [11] showed that in the stretch flanging of TWIP steels, cracking occurs mainly at the grain boundaries between ferrite and martensite, and that grain refinement can improve stretch flangeability. Choi et al. [12] stretch flanged three different types of steel sheets and showed that the alternation of FCC and BCC layers in the steel resulted in lower stretch flangeability due to voids at the phase interfaces. Wang et al. [13] improved the stretch flangeability of TRIP steel by annealing the steel to generate a banded structure of soft ferrite phases, which caused cracks to propagate in the rolling direction.



A schematic illustration of crack initiation in a stretch flanging is shown in Fig. 1. In stretch flanging, a tensile stress is generated at the blank edge, which is deformed in bending. If the roughness of the sheared edge is large, cracks will occur in the product after stretch flanging, triggered by cracks at the blank edge. If the cracks penetrate, the product will be defective, so it is necessary to stretch flange the product to prevent the cracks from penetration. Since the presence of cracks on sheared surfaces increases the potential for crack penetration, it is important to investigate the formation of cracks by shear and their expansion by stretch flanging.

In this paper, the sheared edges of ultra-high-strength blanks sheared at different shear angles were investigated, and the size of the cracks when stretch-flanged was observed.

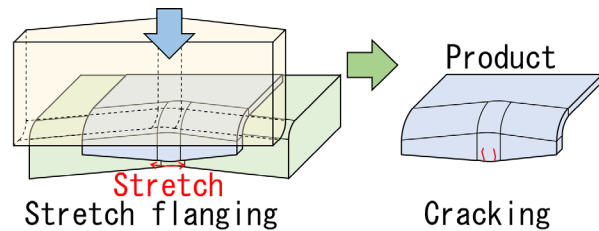


Fig. 1. Crack initiation in stretch flanging.

## Materials and Methods

The mechanical properties of the sheet measured by uniaxial tension test are shown in Table 1. The sheet that the nominal tensile strength was 980 MPa was used. Steel sheet was galvanized alloy zinc (GA) steel sheet. The nominal thickness was 1.2 mm.

Table 1. Mechanical properties of steel sheets.

Steel sheets	Thickness [mm]	Galvannealed	Tensile strength [MPa]	Elongation [%]	Reduction in area [%]	$n$ -value [-]
980 MPa	1.20	Yes	1003	14.1	58.5	0.128

The method of measuring cracks in the stretch flanging of a sheared steel sheets is shown in Fig. 2. A 150 mm wide steel sheet was sheared to an appropriate length, and the sheared edges were observed. The sheared steel sheets were then stretch flanged, and cracks were observed at the bending deformed edges.

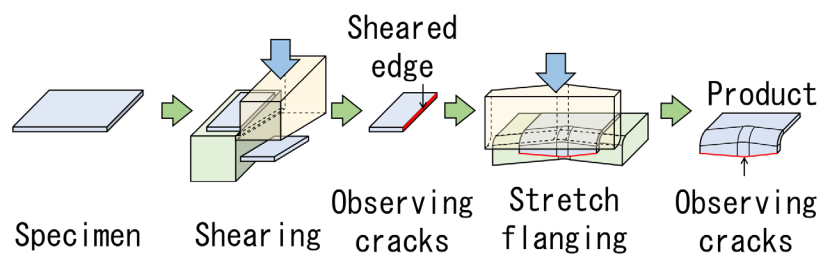


Fig. 2. Method of measuring cracks in stretch flanging of sheared steel sheets.

Shearing conditions are shown in Fig. 3. Each steel sheet was sheared by a die mounted on a servo press (AMADA, SDE-8018). The mean punch speed was 90 mm/s, the shear angles of the punches  $\alpha$ , were 0.0, 0.5, and 1.5°, and the clearance between the punch and die was 0.12 mm. The steel sheets were fixed to the die by a blankholder bolted to the die. Counter blocks of urethane rubber (Shore hardness A90) were attached to the under the punch to prevent steel sheets from dropping.

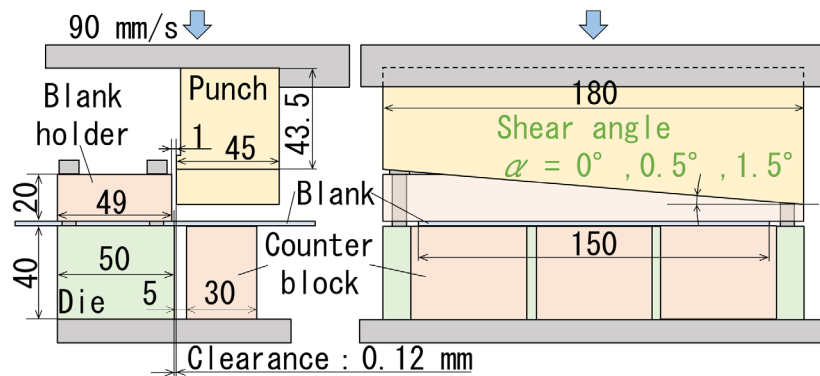


Fig. 3. Shearing conditions.

Stretch flanging conditions are shown in Fig. 4. Each steel sheet was stretch flanged by a die mounted on a servo press (AMADA, SDE-1522). The punch and die had a center angle of  $155^\circ$ , the center was rounded at R50, and the clearance was 1.32 mm. The maximum distance between the sheared edges of the steel sheets and the center of the die was defined as the bend length  $l$ . The steel sheets were formed in 5 mm increments from 15 mm to 45 mm.

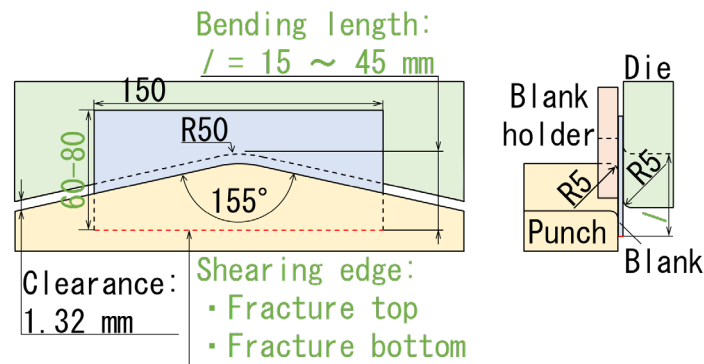


Fig. 4. Stretch flanging conditions.

The steel sheets were mounted on the die by blankholders bolted to the die under two conditions: the fracture top side, where the fracture surface was inside the bend, and the fracture bottom side, where the fracture surface was outside the bend. Anti-rust oil was used as the lubricant.

## Results

**Sheared Edges of Steel Sheets.** The shearing load - punch stroke curve is shown in Fig. 5. The peak shearing load increases with decreasing shear angle, whereas the total stroke decreases.

The sheared edges are shown in Fig. 6(a) to 6(c), and the qualities of sheared edges of sheared sheets are summarized in Fig. 6(d). The sheared edges consisted of the rollover, the burnished surface, and the fracture surface. The ratio of burnished surface was increased by shearing with the punch with shear angle, i.e. the ratio of fracture surface was

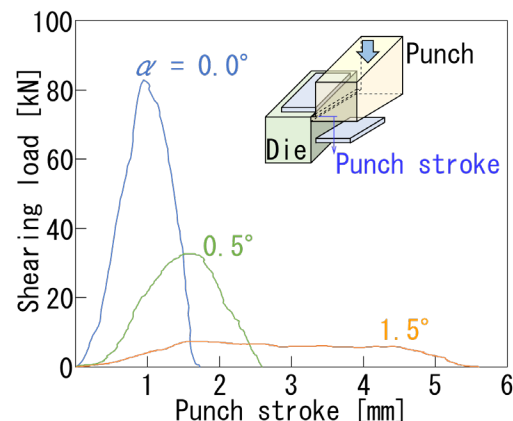


Fig. 5. Shearing load - punch stroke curve.

decreased. In particular, the burnished surface ratio was highest at  $\alpha = 0.5^\circ$ .

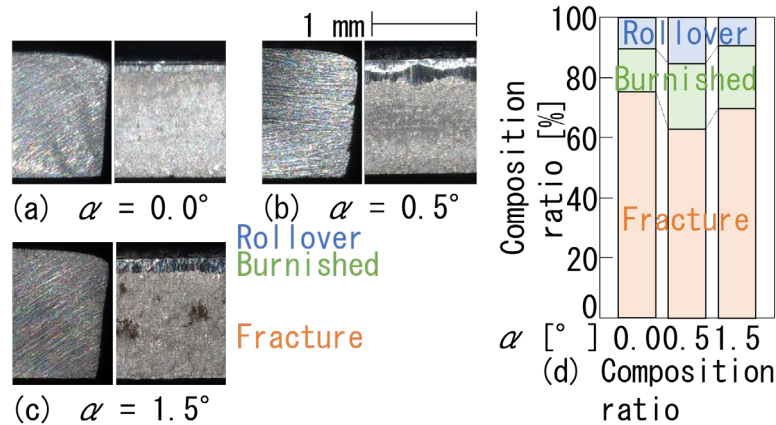


Fig. 6. Sheared edges and quality of sheared edge of sheared sheet.

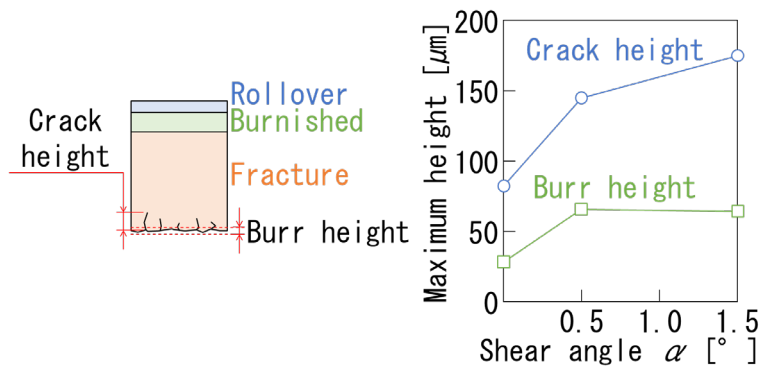


Fig. 7. Maximum crack height and burr height.

In the fracture surface of the sheared edges, cracks that extend into the inside of the fracture surface and small burrs at the edges of the fracture surface were observed. The crack height was defined as the length of the crack from the bottom edge of the fracture surface. The burr height was the length of the burr from the sheet bottom surface. The maximum crack height and burr height sheared at each shear angles are shown in Fig. 7, and the number of cracks per unit width was shown in Fig. 8. The maximum crack height and burr height in the sheared edge with the punch having the shear angle were larger than those in the sheared edge in  $\alpha = 0.0^\circ$ . The cracks per unit width in  $\alpha = 0.5^\circ$  was the largest.

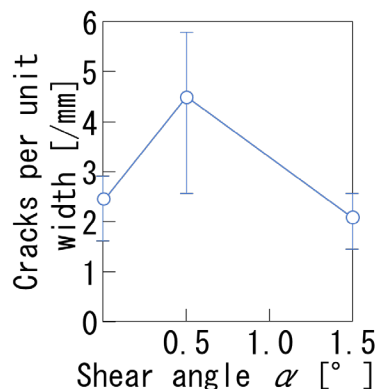


Fig. 8. Number of cracks per unit width.

The boundary edges between the burnished and fractured surfaces of the sheared edge are shown in Fig. 9. The burnished surfaces with the punch having the shear angle were rougher. The boundary edge between the burnished and fractured surfaces was rough with a punch having the shear angle  $\alpha = 0.5^\circ$ .

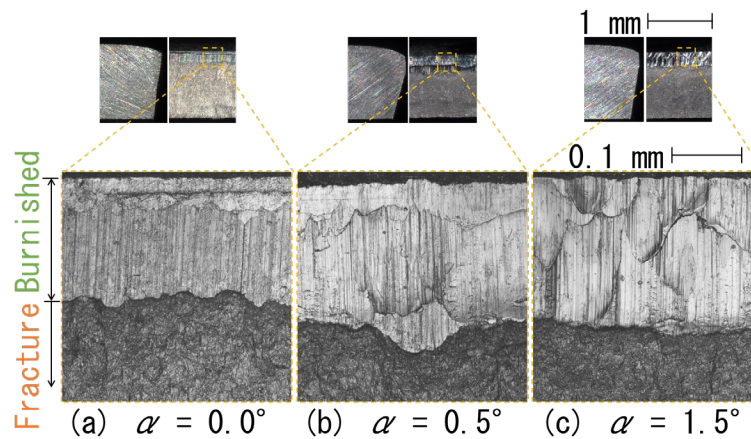


Fig. 9. Boundary between burnished and fractured surfaces.

Cracks after stretch flanging. The stretch flanging ratio with  $\alpha = 0.0^\circ$ , the fracture bottom and  $l = 45$  mm is shown in Fig. 10. The stretch flanging ratio was calculated by the difference of gage length on the blank before and after stretch flanging. The initial gage length  $s$  was 2 mm. The stretch flanging ratio was the largest at the center of the blank, and deformation was concentrated in a range of approximately -15 mm to +15 mm from the center.

The definition of the crack height after stretch flanging is shown in Fig. 11. Cracks were observed at the bending center of the stretch flanging, and the maximum crack height was classified into the following three types;

- No cracks: crack height less than 100  $\mu\text{m}$ ,
- Cracking: crack height larger than 100  $\mu\text{m}$  that do not penetrate in the thickness direction,
- Penetration: cracks penetrating in the direction of the sheet thickness.

Cracks were further classified into two types with a threshold value of 300  $\mu\text{m}$  (1/4 of the sheet thickness).

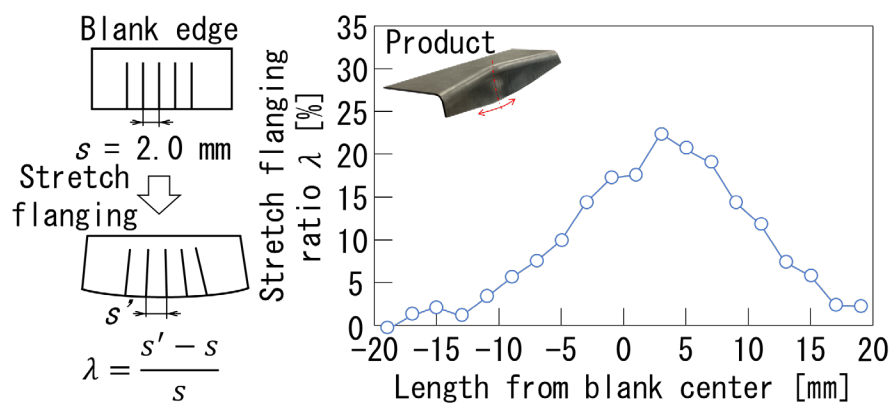
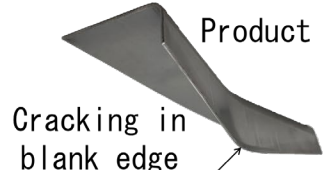


Fig. 10. Stretch flanging ratio with  $\alpha = 0.0^\circ$ , fracture bottom side and  $l = 45$  mm.



Cracking in blank edge

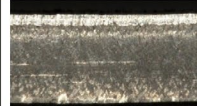

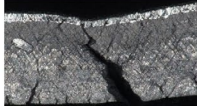
Pattern	No cracks	Cracking	Penetration
Blank edges			
Crack height	$\bigcirc \leq 100 \mu\text{m}$	$\square < 300 \mu\text{m}$ $\triangle \geq 300 \mu\text{m}$	$\times$ Cracks penetration

Fig. 11. Definition of crack height after stretch flanging.

The crack heights after stretch flanging on the fracture top and bottom sides are shown in Fig. 12. For both the conditions, as the bending length increased, the crack heights in the sheared edges increased at  $\alpha = 0.0^\circ$  and  $1.5^\circ$ , although the cracks did not penetrate. On the other hand, the increment of crack height at  $0.5^\circ$  was small. The crack height after stretch flanging was affected by the sheared edge cut by the punch with the shear angle.

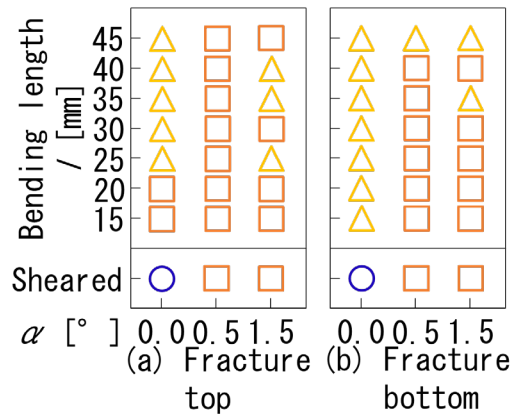


Fig. 12. Crack heights after stretch flanging on the fracture top and bottom sides.

The maximum crack heights for each shear angle after stretch flanging are shown in Fig. 13. A maximum crack height in the sheared edge after stretch flanging was measured in each bending length. On the fracture top side, the maximum crack heights tended to increase as the bending length increased, especially in  $\alpha = 0.0^\circ$  and  $1.5^\circ$ . On the fracture bottom side, the maximum crack height was large in  $\alpha = 0.0^\circ$ , whereas, the height did not increase significantly. On the other hand, in  $\alpha = 0.5^\circ$  and  $1.5^\circ$ , the maximum crack heights increased with increasing bending length, especially at  $l = 45\text{mm}$  where the crack extended significantly in  $\alpha = 1.5^\circ$ . It seems that the maximum crack height and the increment of the height in  $\alpha = 0.5^\circ$  were small, although the increment was depending on the sheared edge and the bending side.



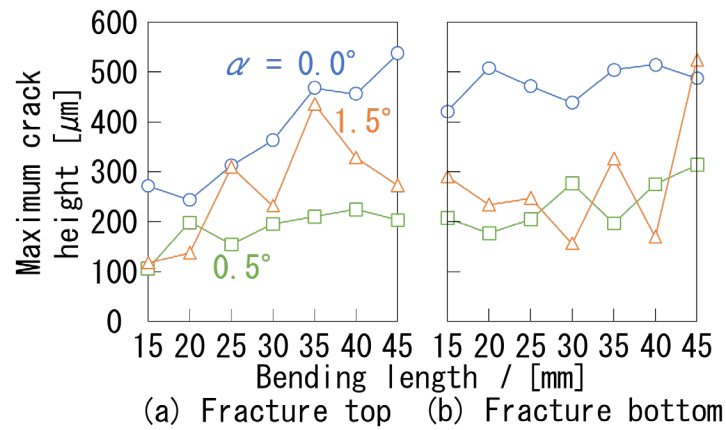


Fig. 13. Maximum crack heights for each shear angle.

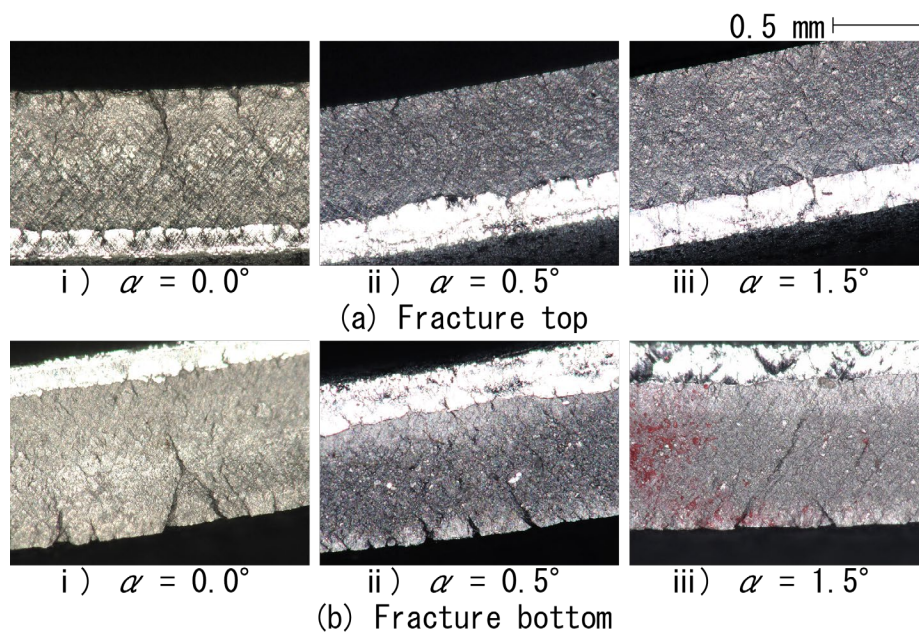


Fig. 14. Edge cracks after stretch flanging with  $l = 45 \text{ mm}$ .

The edge cracks after stretch flanging for each shear angle at  $l = 45 \text{ mm}$  are shown in Fig. 14. Not only in the fracture surface but also in the boundary portion between the burnished and fractured surfaces, the cracks occurred. Although the large cracks with small number are observed in  $\alpha = 0.0^\circ$  and  $1.5^\circ$ , the small cracks with large number in fracture surface are observed in  $\alpha = 0.5^\circ$ . It seems that a large number of initial cracks as shown in Fig. 8 in the sheared edge distributed the deformation in stretch flanging, and then the occurrence of the large crack was prevented.

### Summary

In this paper, the edges of ultra-high-strength blanks sheared with three different shear angles were investigated, and then the size and growth of the cracks in the sheared edge after stretch flanging were observed, with the following results:

- 1) The ratio of burnished surface was increased by shearing with the punch with shear angle, i.e. the ratio of fracture surface was decreased, and in particular, the burnished surface ratio was highest in the shear angle of  $0.5^\circ$ .
- 2) The crack height increase after stretch flanging was suppressed in the shear angle of  $0.5^\circ$  in both the fracture top and bottom sides.

- 3) It seemed that the maximum crack height and the crack increment in the shear angle of  $0.5^\circ$  after stretch flanging were small, although the increment of the maximum crack height was depending on the sheared edge and the bending side.
- 4) It seemed that a large number of cracks are effective in suppressing penetration cracking caused in stretch flanging, because the stretch flangeability increased in the shear angle of  $0.5^\circ$ , where the number of cracks per unit length were the largest.

## References

- [1] M.S. Billur, T. Altan, Challenges in forming advanced high strength steels, *Proc. New Developments in Sheet Metal Forming* (2012) 285-304.
- [2] K. Mori, K. Akita, Y. Abe, Springback behaviour in bending of ultra-high-strength steel sheets using CNC servo press. *Int. J. Mach. Tools Manuf.* 47 (2007) 321-325. <https://doi.org/10.1016/j.ijmachtools.2006.03.013>
- [3] M. Kaupper, M. Merklein, Bendability of advanced high strength steels - A new evaluation procedure, *CIRP Annals - Manuf. Technol.* 62 (2013) 247-250. <https://doi.org/10.1016/j.cirp.2013.03.049>
- [4] Y. Abe, T. Ohmi, K. Mori, T. Masuda, Improvement of formability in deep drawing of ultra-high strength steel sheets by coating of die, *J. Mater. Process. Technol.* 214 (2014) 1838-1843. <https://doi.org/10.1016/j.jmatprotec.2014.03.023>
- [5] K. Mori, Y. Abe, K. Sedoguchi, Delayed fracture in cold blanking of ultra-high strength steel sheets, *CIRP Annals - Manuf. Technol.* 68 (2019) 297-300. <https://doi.org/10.1016/j.cirp.2019.04.111>
- [6] R. Yagita, Y. Abe, Y. Munesada, K. Mori, Deformation Behaviour in Shearing of Ultra-High Strength Steel Sheets under Insufficient Blankholding force, *Procedia Manuf.* 50 (2020) 26-31. <https://doi.org/10.1016/j.promfg.2020.08.006>
- [7] S. Nasheralahkami, W. Zhou, S. Golovashchenko, Study of Sheared Edge Formability of Ultra-High Strength DP980 Sheet Metal Blanks, *J. Manuf. Sci. Eng.* 141 (2019) 091009. <https://doi.org/10.1115/1.4044098>
- [8] Y. Abe, R. Yonekawa, K. Sedoguchi, K. Mori, Shearing of ultra-high strength steel sheets with step punch, *Procedia Manuf.* 15 (2018) 597-604. <https://doi.org/10.1016/j.promfg.2018.07.283>
- [9] P. Sartkulvanich, B. Kroenauer, R. Golle, A. Konieczny, T. Altan, Finite element analysis of the effect of blanked edge quality upon stretch flanging of AHSS, *CIRP Annals - Manuf. Technol.* 59 (2010) 279-282. <https://doi.org/10.1016/j.cirp.2010.03.108>
- [10] L. Pan, J. Xiong, Z. Zuo, W. Tan, J. Wang, W. Yu, Study of the stretch-flangeability improvement of dual phase steel, *Procedia Manuf.* 50 (2020) 761-764. <https://doi.org/10.1016/j.promfg.2020.08.137>
- [11] H. Gwon, J.H. Kim, J-K. Kim, D-W. Suh, S-J. Kim, Role of grain size on deformation microstructures and stretch-flangeability of TWIP steel, *Mater. Sci. Eng. A* 773 (2020) 138861. <https://doi.org/10.1016/j.msea.2019.138861>
- [12] Y.T. Choi, P. Asghari-Rad, J.W. Bae, H.S. Kim, Effect of phase interface on stretch-flangeability of metastable ferrous medium-entropy alloys, *Mater. Sci. Eng. A* 852 (2022) 143683. <https://doi.org/10.1016/j.msea.2022.143683>
- [13] Y. Wang, Y. Xu, X. Wang, J. Zhang, F. Peng, X. Gu, Y. Wang, W. Zhao, Improving the stretch flangeability of ultra-high strength TRIP-assisted steels by introducing banded structure, *Mater. Sci. Eng. A* 852 (2022) 143722. <https://doi.org/10.1016/j.msea.2022.143722>